PNAS RESEARCH ARTICLE | BIOCHEMISTRY

Impact of acute stress on murine metabolomics and metabolic flux

Won Dong Lee[a,b,c], Lingfan Liang[a,b,c], Jenna AbuSalim[b,c,d], Connor S.R. Jankowski[b,c,d], Laith Z. Samarah[a,b,c], Michael D. Neinast[a,b,c], and Joshua D. Rabinowitz[a,b,c,d,1]

Edited by C. Ronald Kahn, Harvard Medical School, Boston, MA; received January 23, 2023; accepted April 10, 2023

Plasma metabolite concentrations and labeling enrichments are common measures of organismal metabolism. In mice, blood is often collected by tail snip sampling. Here, we systematically examined the effect of such sampling, relative to gold-standard sampling from an in-dwelling arterial catheter, on plasma metabolomics and stable isotope tracing. We find marked differences between the arterial and tail circulating metabolome, which arise from two major factors: handling stress and sampling site, whose effects were deconvoluted by taking a second arterial sample immediately after tail snip. Pyruvate and lactate were the most stress-sensitive plasma metabolites, rising ~14 and ~5-fold. Both acute handling stress and adrenergic agonists induce extensive, immediate production of lactate, and modest production of many other circulating metabolites, and we provide a reference set of mouse circulatory turnover fluxes with noninvasive arterial sampling to avoid such artifacts. Even in the absence of stress, lactate remains the highest flux circulating metabolite on a molar basis, and most glucose flux into the TCA cycle in fasted mice flows through circulating lactate. Thus, lactate is both a central player in unstressed mammalian metabolism and strongly produced in response to acute stress.

metabolomics | isotope tracing | stress | catecholamine | in vivo

Plasma metabolite profiling has provided insights into physiology in health and disease, and biomarkers for disease diagnosis and prognosis (1–6). Measurement of arteriovenous metabolite concentration differences has revealed organ-specific metabolite production and consumption (7–9). Tracking plasma metabolite labeling from radioactive or stable isotope tracers has revealed pathway activities and whole-body nutrient turnover rates (10–12).

Conscious arterial blood sampling from a preimplanted catheter is the gold standard for assessing circulating metabolites in mammals, as organs are fed by arterial blood, and drawing blood from a preimplanted catheter avoids the handling stress (13–15). Such sampling, however, requires surgery for catheter implantation, for mice typically in the carotid artery, and murine blood sampling from the tail tip has been widely used as an alternative.

Despite the common practice of tail-tip sampling, there is no definitive reference concerning its impact on metabolite measurements (16). Here, we examined the effect of arterial catheter versus tail snip sampling on plasma metabolomics and stable isotope tracing. We find substantial differences between arterial and tail circulating metabolome, which we dissect into two major components, one induced by handling stress and the other related to the sampling site. Using stable isotope tracing, we show that stress induces production of several metabolites, most strongly pyruvate and lactate, and we provide a reference set of mouse circulatory turnover fluxes measured with minimal stress by noninvasive arterial sampling.

Results

Effects of Stress and Sampling Site on Plasma Metabolite Concentrations. For conscious arterial sampling, a catheter was surgically implanted in the left carotid artery, and mice were allowed to recover before experiments. The catheter was connected to tubing via swivel and tether to allow the mouse to move freely around the cage and samples to be collected noninvasively (Fig. 1*A*). After a 6-h fast, arterial blood (Artery 1) was drawn through the carotid artery catheter (without the experimenter in any way perturbing the mouse cage), followed by a tail snip sampling (Tail) and collection of a second arterial sample immediately thereafter (Artery 2) (17, 18).

We first investigated the global similarity in the metabolome of the arterial and tail plasmas. Principal component analysis (PCA) showed that metabolic profiles of the pretail-snip and posttail-snip arterial plasmas were more similar to each other than to that of the tail plasma (Fig. 1*B* and Datasets S1). Comparing arterial and tail plasma (Artery 1 vs Tail),

Significance

Here we show that blood sampling can impact measured metabolite levels both via the location of the sampling site and via acute stress. The impact of the sampling stress manifests primarily in two central metabolites: pyruvate and lactate. Stress-induced production from both glucose and glycogen increases these metabolites' levels several-fold within seconds of stress or adrenergic activation. Such production makes energy via glycolysis. The resulting elevated blood levels provide enhanced circulating fuel to power, via oxidative metabolism, the fight-or-flight response.

Author affiliations: [a]Department of Chemistry, Princeton University, Princeton, NJ 08544; [b]Lewis-Sigler Institute for Integrative Genomics, Princeton University, Princeton, NJ 08544; [c]Ludwig Institute for Cancer Research, Princeton University, Princeton, NJ 08544; and [d]Department of Molecular Biology, Princeton University, Princeton, NJ 08544

Author contributions: W.D.L., M.D.N., and J.D.R. designed research; W.D.L., L.L., J.A., C.S.R.J., and L.Z.S. performed research; W.D.L., L.L., J.A., C.S.R.J., and L.Z.S. analyzed data; and W.D.L. and J.D.R. wrote the paper.

Competing interest statement: J.D.R. is an advisor and stockholder in Colorado Research Partners, L.E.A.F. Pharmaceuticals, Bantam Pharmaceuticals, Barer Institute, and Rafael Pharmaceuticals; a paid consultant of Pfizer and Third Rock Ventures; a founder, director, and stockholder of Farber Partners, Serien Therapeutics, and Sofro Pharmaceuticals; a founder and stockholder in Empress Therapeutics; inventor of patents held by Princeton University; and a director of the Princeton University-PKU Shenzhen collaboration.

This article is a PNAS Direct Submission.

[1]To whom correspondence may be addressed. Email: joshr@princeton.edu.

This article contains supporting information online at https://www.pnas.org/lookup/suppl/doi:10.1073/pnas.2301215120/-/DCSupplemental.

Published May 15, 2023.

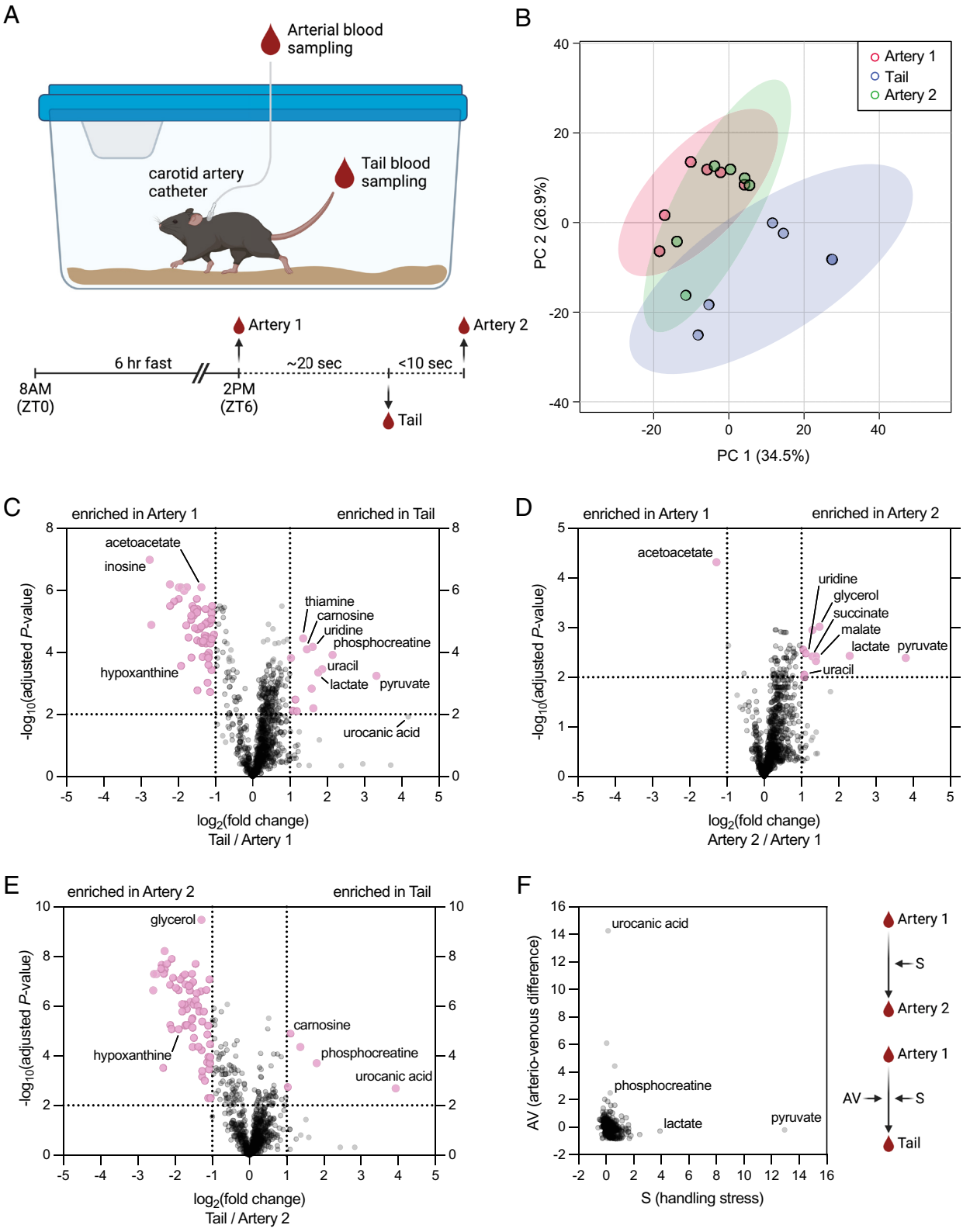

Fig. 1. Stress and sampling site change plasma metabolite concentrations. Data are from 6-h fasted mice. (*A*) Experimental scheme. (*B*) Principal component analysis of untargeted metabolomics data from plasma collected from the arterial catheter and tail snip ($n = 6$). Arterial sampling (Artery 1) was followed by tail snip sampling (Tail) and an immediate second arterial sampling (Artery 2). (*C*) Volcano plot of metabolite abundance in Tail relative to Artery 1. (*D*) Volcano plot of metabolite abundance in Artery 2 relative to Artery 1. (*E*) Volcano plot of metabolite abundance in Tail relative to Artery 2. (*F*) Linear model of the effect of handling stress (*S*) and arteriovenous difference (AV) on metabolite concentrations in Tail relative to Artery 1. *P*-values were derived from the Welch *t* test and then Benjamini–Hochberg corrected (adjusted *P*-value). The horizontal dotted line indicates adjusted *P*-value = 0.01. The vertical dotted line indicates a twofold change in metabolite concentration. Data are mean, $n = 10$ mice (*C*–*F*).

among 868 metabolites examined, 74 (~9%) changed statistically significantly and by more than twofold (adjusted *P*-value < 0.05) (Fig. 1*C* and Table 1 and Dataset S2).

We hypothesized that metabolic differences between the initial arterial sample and tail sample reflect two primary factors: i) systemic metabolic changes due to handling stress (e.g., acute

Table 1. Absolute nutrient concentrations in mice fasted for 6 to 8 h as measured with sampling from the arterial catheter (without sampling stress) versus tail snip

	Plasma concentration (μM)					
	Artery			Tail		
Metabolite	MEAN	SEM	N	MEAN	SEM	N
Glucose	7,704	299	6	7,985	534	10
Lactate***	970	28.9	6	3,279	324	10
3-hydroxybutyrate	494	67.1	6	369	61.9	10
Glutamine*	363	8.83	6	424	21.1	10
Citrate	295	35.8	6	394	50.7	10
Creatine	282	19.8	6	322	24.4	10
Alanine*	202	8.36	6	246	17.0	10
Lysine	168	11.6	6	199	16.7	10
Valine	155	18.3	6	153	20.5	10
Glycine	148	9.57	6	169	13.7	10
a-ketoglutarate	133	18.5	6	202	30.8	10
Leucine	98.2	9.19	6	93.4	11.5	10
Threonine	77.8	7.93	6	76.5	8.91	10
Isoleucine	67.0	8.29	6	62.4	9.15	10
Serine	51.5	2.05	6	53.3	4.33	10
Arginine	46.9	3.42	6	55.5	5.66	10
Phenylalanine	43.0	1.77	6	48.9	3.90	10
Proline	41.5	2.42	6	45.1	3.49	10
Tyrosine	39.2	4.90	6	44.6	7.08	10
Tryptophan	35.8	3.20	6	50.9	7.74	10
Aspartate*	33.6	4.01	6	79.0	18.0	10
Histidine	31.2	1.87	6	35.0	2.96	10
Methionine	27.3	1.90	6	28.7	2.44	10
Glutamate	16.4	1.39	6	22.0	2.42	10
Asparagine	15.6	0.883	6	15.5	1.29	10
Malate*	12.4	1.26	6	20.0	2.26	10
Succinate***	10.7	0.847	6	20.0	1.97	10

*$P < 0.05$.
**$P < 0.01$.
***$P < 0.001$ by the Welch t test.

adrenergic response) and ii) local differences in sampling site (e.g., arteriovenous differences due to local tail metabolism, metabolites released from damaged tail muscle). To probe the effect of handling stress, we performed a systemic comparison between the arterial samples taken before and after the tail sampling (Fig. 1*D* and Dataset S2). Pyruvate and lactate showed the strongest changes, increasing ~14 and ~5-fold, respectively.

Similarly, to address the effect of sampling site, we compared Tail and Artery 2 samples (Fig. 1*E* and Dataset S2). Urocanic acid, phosphocreatine, and carnosine were highly concentrated in the tail snip sample, which is consistent with the fact that these metabolites are abundant in skin and muscle (19–22). Many other metabolites were depleted in the tail snip sample, consistent with their being consumed by tail metabolism. A linear model was used to quantify the relative effect sizes of handling stress (S) and arteriovenous difference (AV) on individual plasma metabolites (Fig. 1*F* and Dataset S3). Pyruvate and lactate were the most stress-sensitive metabolites, while urocanic acid and phosphocreatine were tail-specific.

Circulatory Fluxes Measured by Arterial Sampling. Circulating metabolite fluxes (endogenous production rates or Ra) are measured by infusing isotope-labeled metabolites and monitoring their resulting labeling in the bloodstream (11). We assessed whether such measurements are impacted by stress and sampling site. Since metabolomics suggested stress-induced lactate production, we first infused ^{13}C-lactate and measured the labeling enrichment in arterial and tail blood. In this experiment, flux is based on the dilution of the infused tracer, so low labeling implies high flux. Note that when carbon-labeled lactate tracers are used to quantitate lactate flux, exchange between lactate, pyruvate, and alanine does not alter lactate's carbon skeleton and thus does not contribute to observed circulatory turnover flux (23, 24). Lactate showed a strong decrease in tracer enrichment in both the tail blood and second arterial samples, indicating that handling stress results in acute and more than doubled production flux of this metabolite (Fig. 2*A*). Dilution in the tail was yet greater than in the second arterial sample, arguing for stress-induced release occurring in part in the tail.

Given the large effect on lactate flux, we carried out similar experiments with other circulating carbon carriers. Glucose and glycerol showed modest decreases in tracer labeling in the second arterial samples, indicating subtle enhancement of endogenous production by handling stress (Fig. 2 *B* and *C*). This occurred without substantial dilution in the tail samples, supporting stress-induced release elsewhere in the body, presumably liver for glucose and adipose for glycerol. Glutamine and leucine tracing was insensitive to handling stress with a subtle effect of sampling

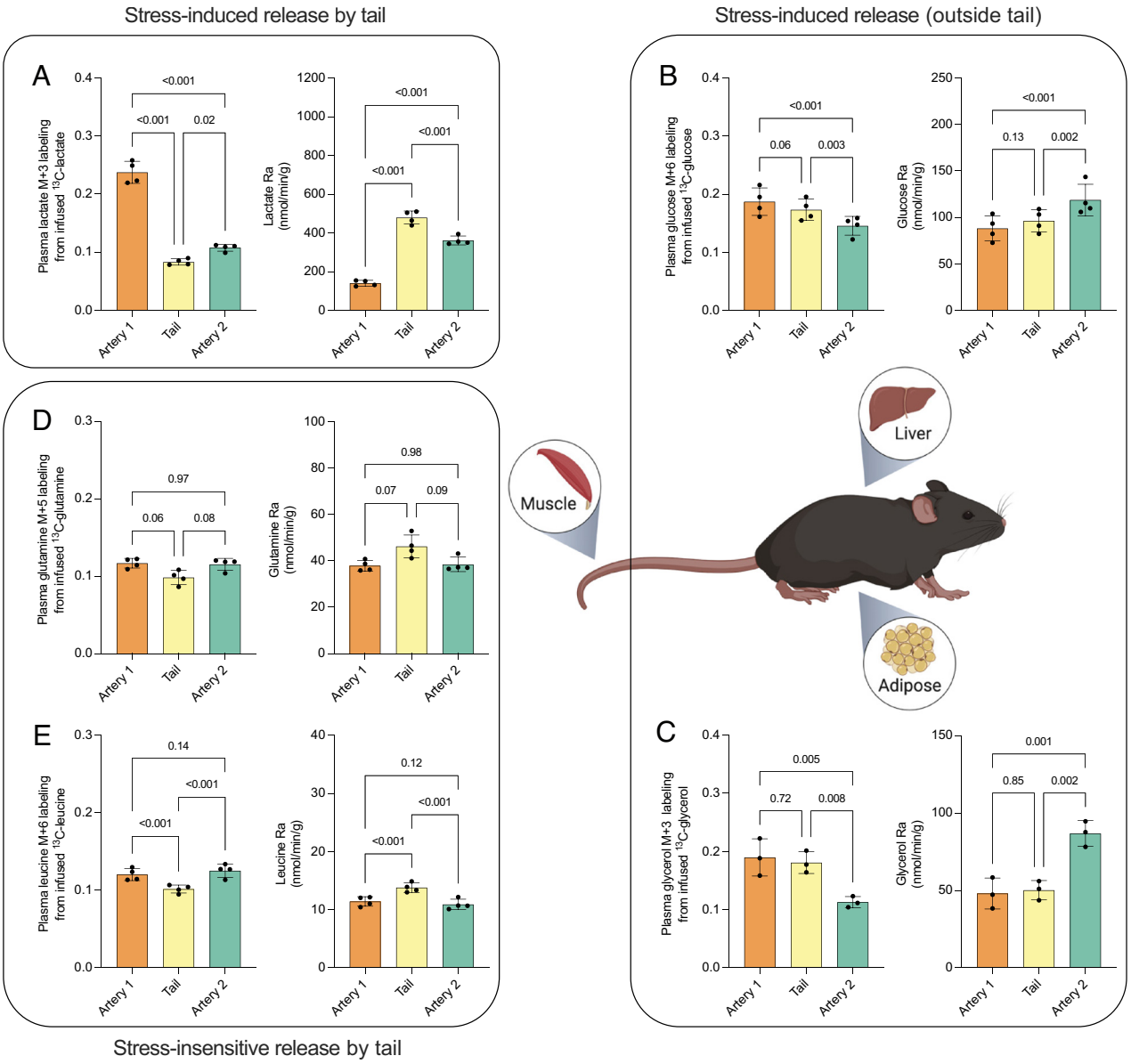

Fig. 2. Stress induces systemic and local metabolite production. Data are from mice fasted for 6 to 8 h. Steady-state plasma labeling enrichments and production fluxes of lactate (*A*), glucose (*B*), glycerol (*C*), glutamine (*D*), and leucine (*E*). Arterial sampling (Artery 1) was followed by tail snip sampling (Tail) and an immediate second arterial sampling (Artery 2). Repeated measures one-way ANOVA. *P*-values for paired sample comparison are adjusted for multiple comparison using Tukey's method. Data are mean ± SEM, *n* = 3 or 4 mice.

site, likely reflecting local production in the tail by protein catabolism (Fig. 2 *D* and *E*).

Based on the discernible effect of sampling on fluxes of all the above metabolites, we systematically measured the turnover fluxes of all abundant circulating metabolites, including amino acids, carboxylic acids, and fatty acids, using noninvasive arterial sampling (Table 2). Compared to prior data using tail snip sampling, many fluxes were modestly lower, and a few substantially so. Replicates showed significantly less variation than prior data (*SI Appendix*, Fig. S1), likely because a major source of measurement error was associated with tail sampling, either due to stress or inhomogeneity of the released fluid from tail. The table of circulatory fluxes measured by arterial sampling provides a physiological reference for the field.

Acute Metabolic Responses to Catecholamines. Metabolic responses to stress occur on different time scales, seconds to minutes for the sympathetic nervous system and hours for the hypothalamic–pituitary axis (25). We monitored the dynamics of arterial plasma metabolite level change after mouse handling (tail snip) (Fig. 3*A* and Dataset S4). Consistent with Fig. 1*D*, the main changes were increased levels of metabolites including lactate, pyruvate, malate, uridine, and nonesterified fatty acids (NEFA). These metabolites rose quickly (within 30 s) with peak levels occurring over the first 5 min and decreasing thereafter (Fig. 3 *A*–*C*). Lactate, NEFA, and glucose have been suggested to represent metabolic responses to acute stress of skeletal muscle, adipose tissue, and liver, respectively (26). Arterial glucose increased less rapidly than most of the other stress-elevated metabolites, peaking at 15 min poststress (Fig. 3*D*). These data suggest that acute stress first induces skeletal muscle glycolysis and adipose tissue lipolysis, thus providing TCA fuels (lactate and NEFA) to other organs while supplying substrates (lactate and glycerol) for liver gluconeogenesis.

Experiments involving catecholamine IV injection (0.1 mg/kg epinephrine or 0.2 mg/kg norepinephrine) with sampling via an arterial catheter (without tail snip or other mouse manipulation)

Table 2. Nutrient turnover fluxes (F_{circ}) in mice fasted for 6 to 8 h as measured with tracer infusion via the jugular vein catheter and sampling from the arterial catheter (without sampling stress) or tail snip

	Fcirc (nmol g^{-1} min^{-1})					
	Artery			Tail		
Metabolite	MEAN	SEM	N	MEAN	SEM	N
Lactate***	151.70	10.17	7	339.34	48.05	36
Glucose	95.41	4.36	8	124.47	14.55	37
Glycerol	48.06	5.77	3	51.77	2.41	6
Linoleate	47.76	4.62	3	45.00	2.00	6
Glutamine	37.89	1.16	4	42.16	4.05	17
Acetate	37.30	3.97	5	56.00	8.00	7
Oleate*	29.48	0.66	3	35.00	2.00	6
3-hydroxybutyrate	27.49	1.97	6	45.74	11.08	20
Alanine*	24.02	1.46	9	45.79	4.69	4
Palmitate	23.96	2.03	3	25.89	8.44	17
Glycine	13.79	0.54	4	20.62	5.23	16
Serine	11.31	0.21	4	28.86	14.95	23
Lysine	10.16	0.89	5	9.61	0.79	13
Leucine	9.93	0.64	9	11.12	1.38	15
Valine	9.89	0.32	5	10.13	3.43	20
Taurine	9.13	0.31	5	9.85	1.06	6
Isoleucine	7.57	0.52	5	7.73	0.87	13
Threonine	6.02	0.45	7	7.31	0.48	13
Tyrosine	5.41	0.46	4	8.00	1.27	3
Citrate***	4.86	0.54	4	11.00	1.00	13
Proline	4.71	0.32	5	5.38	0.86	8
Phenylalanine	4.27	0.33	7	5.60	0.75	13
Methionine	4.15	0.40	5	4.55	0.89	20
Arginine*	4.11	0.22	5	9.32	1.96	15
Glutamate	3.95	0.39	4	–	–	–
a-ketoglutarate	3.42	0.15	5	4.18	0.78	14
Asparagine*	2.94	0.29	5	4.84	0.68	9
Aspartate	2.38	0.42	5	–	–	–
Tryptophan	1.86	0.06	7	1.82	0.19	14
Succinate	1.80	0.22	4	3.10	0.64	3
Histidine	1.77	0.17	5	2.75	0.50	7
Creatine*	1.47	0.09	4	2.60	0.29	3
Malate	1.04	0.10	4	1.92	0.44	9

*$P < 0.05$.
**$P < 0.01$.
***$P < 0.001$ by the Welch *t* test.

resulted in many of the same metabolic effects as tail snipping (Fig. 3 *A–D*). Norepinephrine did not produce as strong or broad-based metabolic changes as tail snip or epinephrine, perhaps due to a role for both beta-1 and beta-2 adrenergic receptor activation in the response to tail snip and epinephrine, while norepinephrine mainly activates beta-1 receptors (27). Tail snip and catecholamine IV injection resulted in similar metabolite kinetics, suggesting that catecholamines are the primary effectors of the time-dependent and tissue-specific responses to acute stress. Catecholamine injection increased the endogenous lactate production flux measured by ^{13}C-lactate infusion, consistent with the role of catecholamines in acute stress response (Fig. 3*E*).

Tissue Metabolite Sources. Tissue metabolite labeling is routinely normalized to circulating tracer enrichment. Accordingly, measurements of tissue metabolite sources are impacted by systematic error in measurements of circulating tracer labeling. Even for metabolites whose tissue labeling is not acutely stress sensitive, stress-induced decreases in the circulating tracer labeling will lead to overestimation of the tracer's contribution to tissue metabolites.

Recently, we have reported that circulating lactate is a major TCA carbon source in almost all tissues (24). Deconvolution of the direct contributions of circulating glucose versus circulating lactate to tissue TCA metabolism revealed lactate as the greater direct fasted-state carbon donor in tissues other than the brain. These analyses were carried out using tail snip blood without taking into consideration the impact of stress on circulating lactate or glucose label enrichment.

We revisited the direct TCA contributions of glucose and lactate with minimally perturbative arterial blood sampling. The

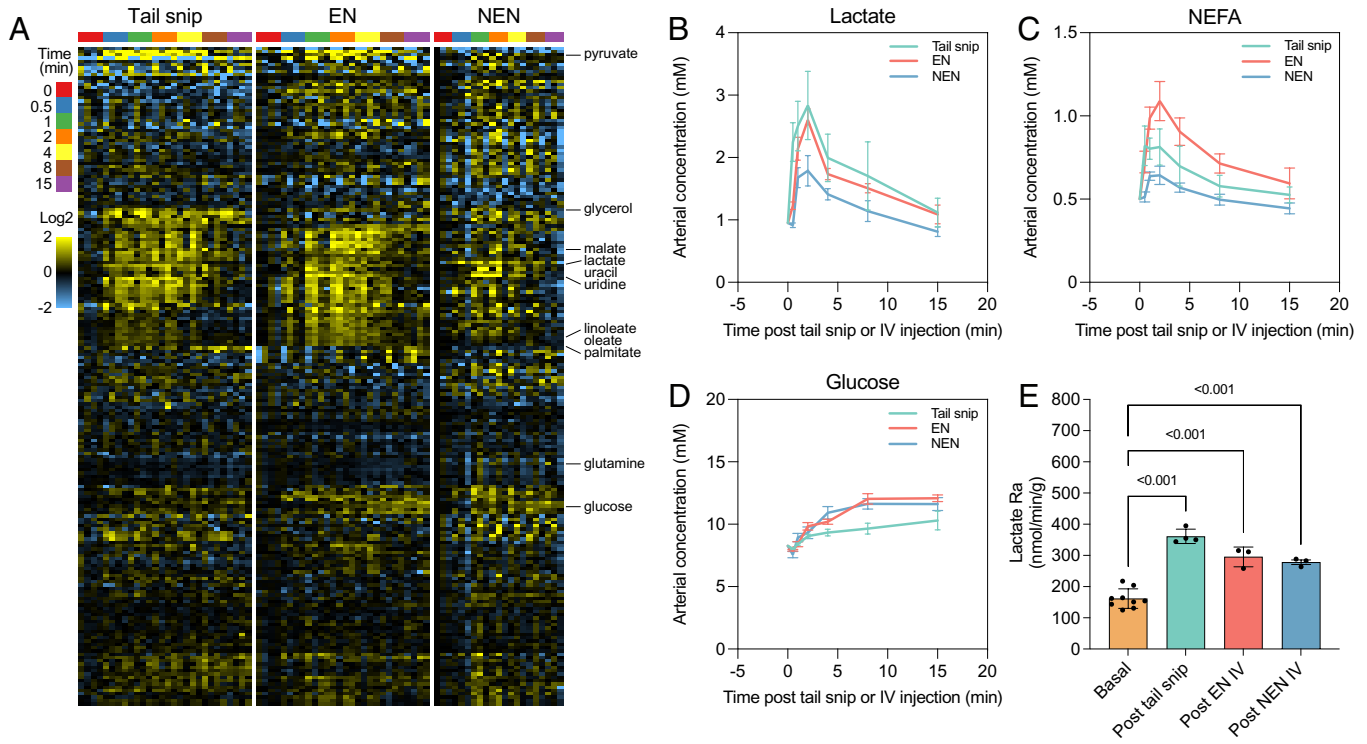

Fig. 3. Catecholamines orchestrate the time-dependent and tissue-specific responses to acute stress. Data are from mice fasted for 6 to 8 h. (*A*) Heatmap of arterial metabolite level relative to basal (log2) after tail snip or catecholamine (0.1 mg/kg epinephrine [EN] or 0.2 mg/kg norepinephrine [NEN]) IV injection (n = 4 for tail snip and EN IV, and n = 3 for NEN IV). The arterial plasma concentrations of lactate (*B*), nonesterified fatty acids (NEFA) (*C*), and glucose (*D*) after tail snip or catecholamine IV injection (n = 4 for tail snip and n = 5 for EN and NEN IV). (*E*) Lactate production flux at basal, 2 min post tail snip, or 2 min post catecholamine (epinephrine or norepinephrine) IV injection. One-way ANOVA. *P*-values for paired sample comparison are adjusted for multiple comparison using Tukey's method. Data are mean ± SEM, n = 9 for basal, n = 4 for tail snip, and n = 3 for EN and NEN IV.

impact of stress on tissue metabolites was minimized by euthanizing mice with pentobarbital given via an arterial catheter without handling the mice. The resulting measurements validate the importance of lactate as a tissue TCA feedstock (Fig. 4*A*). Indeed, the present TCA contribution results align closely with our previously published data from tail snip sampling, even though the prior data were confounded by stress. The similarity arises because those prior measurements were aggressively corrected for potential arterial-venous labeling differences, and the magnitude of those corrections effectively incorporated the impact of both sampling site and handling stress (Fig. 4 and *SI Appendix*, Fig. S2). Analogous measurements in fed mice confirm increased utilization of glucose as a direct tissue TCA nutrient source in the fed state, and identify brain, adipose, and muscle as tissue types with substantial direct fed-state glucose burning (Fig. 4*B*).

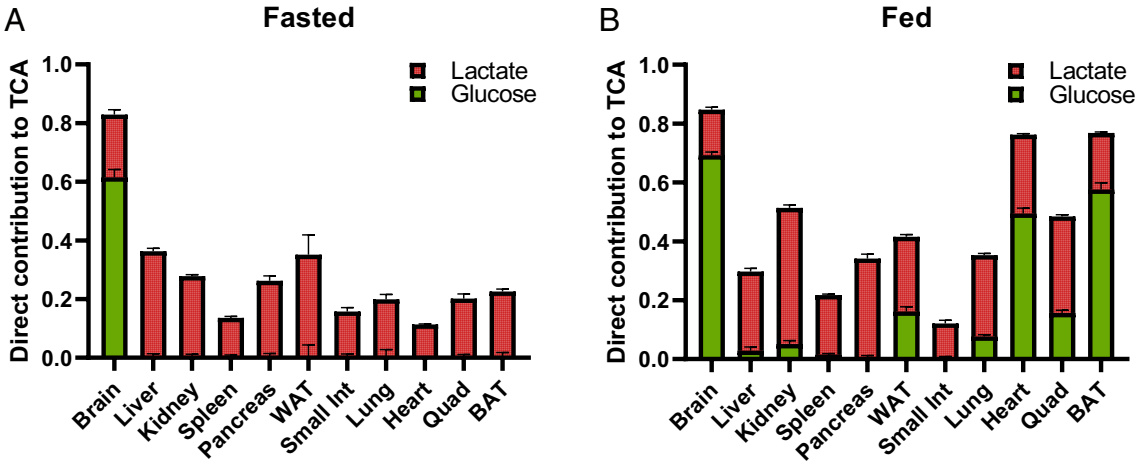

Fig. 4. Circulating lactate and glucose direct contributions to tissue TCA as determined with minimally perturbative arterial blood sampling and euthanasia. The direct contribution of circulating lactate and glucose to tissue TCA intermediates in 6 to 8-h-fasted (*A*) and 4-h ad libitum-fed (*B*) mice. Circulating lactate and glucose labeling was measured through an implanted arterial catheter. Mice were euthanized via pentobarbital delivered via an arterial catheter. Tissue TCA labeling was determined based on the average of malate and succinate. Direct contributions were determined from linear algebra analysis of the resulting TCA metabolite enrichments relative to circulating tracer enrichments. Data are mean ± SEM, n = 16 mice total: 4 each for glucose tracing and for lactate tracing, in both the fed and fasted states.

Discussion

With an implanted arterial catheter and untargeted metabolomics, we found that pyruvate and lactate are the most stress-sensitive metabolites in the circulation. Metabolite dynamics revealed two stages in the acute metabolic response to stress. The first stage, occurring within 2 min, is characterized by increased production and release of pyruvate/lactate and glycerol/NEFAs into the bloodstream, presumably from muscle and adipose, respectively. The second stage, occurring in roughly the following half-hour, is characterized by the recovery of basal pyruvate/lactate and glycerol/NEFA levels and the slow increase of blood glucose, likely due to increased hepatic gluconeogenesis. These data suggest that previously reported short-term stress responses follow a coordinated temporal sequence, involving cross talk between multiple organs (28).

Previously, we reported exceptionally high lactate fluxes in mice based on tail snip sampling, exceeding glucose flux by roughly 2.5-fold on a molar basis (1.2-fold on a carbon atom basis) (24). Based on the present data, these fluxes reflect in part acute stress, and are lower in nonstressed mice. But even in the nonstress basal fasted state, lactate remains the circulating metabolite with the highest flux on a molar basis, exceeding that of glucose by 60% (with glucose having 25% higher flux than lactate on a carbon atom basis). These data yield a coherent picture of metabolism: In the fasted state, most carbohydrate burning occurs via circulating lactate [made typically via muscle glucose catabolism (29)], with a small amount occurring directly from glucose. This aligns with glucose having a slightly larger circulatory flux than lactate on a carbon atom basis. Stress results in acute breakdown of both glucose and glycogen into circulating lactate, roughly doubling the circulating lactate flux (with a slightly lower fraction of circulating lactate coming from circulating glucose and instead presumably from muscle glycogen (*SI Appendix*, Fig. S3). Consistent with this, skeletal muscle is the largest glycogen store in mammals (30) and catecholamines trigger the breakdown of muscle glycogen (31), with liver glycogen used to support fasting glucose homeostasis and muscle glycogen preferentially reserved for acute fight-or-flight responses (32, 33).

In conclusion, plasma metabolites are routinely collected and analyzed to probe metabolic activities in vivo, and care in sampling is needed to capture the unperturbed basal metabolic state. Acute stress can alter plasma metabolite concentrations and labeling enrichments, with many metabolites minimally altered but others (like lactate) highly stress sensitive. For those, blood sampling through an implanted catheter is much preferred.

Materials and Methods

Animals. Animal studies followed protocols approved by the Princeton University Institutional Animal Care and Use Committee. All experiments were performed on 10 to 14-wk-old C57BL/6 male mice precatheterized in the right jugular vein and left carotid artery (Charles River Laboratories). Upon arrival, precatheterized mice were acclimated to the mouse facility for at least 3 d (72 h) prior to use. Mice with catheters were individually housed in environmentally enriched (Bed-r'Nest®, The Andersons) cages with ad libitum access to water and food. Catheters were flushed with sterile saline and refilled with sterile heparin glycerol locking solution (SAI, HGS) every 5 to 6 d. Animals were housed on a normal light cycle (8 AM to 8 PM) and fed a standard rodent chow (PicoLab Rodent 20 5053, St. Louis, MO) provided on the floor.

Blood Sampling for Untargeted Metabolomics. One day before the experiment, catheters were flushed with sterile saline and refilled with sterile heparin saline locking solution (SAI, HS10) to remove lock solution glycerol. On the day of the experiment, mice were transferred to new cages with enrichment (The Andersons, Bed-r'Nest) and water gel (ClearH_2O, HydroGel) but without food around 8 AM (beginning of the light cycle). To minimize excess noise, vibrations, and other disturbances, mice cages were transferred to a quiet and isolated procedure room and placed on a firm table maintaining some space between them and walls. Catheters were flushed with sterile saline. The experimenter left the room and let the mice acclimate to the new environment. Around 1 PM, catheters were flushed again with sterile saline, and mice were weighed and connected to infusion lines with swivel and tether (Instech products: swivel SMCLA, line KVABM1T/25) that allowed the animals to have free movement in the cage. Arterial and venous infusion lines were prefilled with heparinized saline (10 U/mL) and saline, respectively, before connecting to the catheters. The experimenter left the room and mice were left in cages connected to lines for 1 h to reduce stress. Around 2 PM, a predetermined dead volume (70 μL) was withdrawn from the arterial infusion line and arterial blood (10 μL) was sampled from the arterial catheter using a capillary blood collection tube coated with lithium heparin (Sarstedt 41.1503.105). The arterial infusion line was refilled with the withdrawn dead volume (70 μL). First arterial blood sampling (Artery 1) was followed by a tail snip sampling (Tail) and an immediate second arterial sampling (Artery 2). For kinetic metabolite profiling, arterial blood was sampled from the arterial catheter at 0, 0.5, 1, 2, 4, 8, and 15 min post tail snip or catecholamine (0.1 mg/kg epinephrine [EN] or 0.2 mg/kg norepinephrine [NEN]) IV injection. The length of the tail snips was 1 ~ 2 mm. To avoid both trauma and adaptation to handling stress, tail snip sampling was performed once per mouse. Blood samples were stored on ice and then centrifuged at 10,000 × g for 10 min at 4 °C to get plasma samples. Plasma samples were kept at −80 °C until LC-MS analysis.

Stable Isotope Tracer Infusion. To measure steady-state plasma labeling enrichments and nutrient turnover rates, stable isotope tracers were infused for 2.5 h through the implanted right jugular vein catheter. For glycerol measurements, the catheter locking solution (SAI, HGS), which contains 50% glycerol, was replaced with a glycerol-free locking solution (SAI, HS10) a day before the experiment, and catheters were flushed twice in the morning of the experiment. The same fasting and sampling procedure was performed after the tracer infusion. For ad libitum fed experiments, mice were weighted and connected to infusion lines with swivel and tether around 8 PM (beginning of the dark cycle). Around 9:30 PM, stable isotope tracers were infused for 2.5 h, and samples were collected around midnight as described above.

Catecholamine IV Injection. To measure the effect of catecholamines on circulating metabolite concentrations and turnover, epinephrine (0.1 mg/kg) or norepinephrine (0.2 mg/kg) was injected through the implanted right jugular vein catheter. Epinephrine injection 1 mg/mL (Vedco Inc.) and norepinephrine bitartrate Injection, USP, 1 mg/mL (Covetrus) were diluted in sterile saline to obtain a 0.1 and 0.2 mg/mL working solutions, respectively. For a 25-g mouse, 25 μL 0.1 mg/mL epinephrine or 0.2 mg/mL norepinephrine solution was injected through the implanted right jugular vein catheter, using a syringe pump (NE-1000, New Era Pump Systems Inc.) set at 200 μL/min. Blood samples were collected at 0, 0.5, 1, 2, 4, 8, and 15 min post catecholamine injection.

Plasma Metabolite Extraction. Plasma (2.5 μL) was added to 60 μL −20 °C 25:25:10 (v/v/v) acetonitrile:methanol:water solution, vortexed for 10 s, and put on ice for at least 5 min. The resulting extract was centrifuged at 21,000 × g for 20 min at 4 °C and supernatant was transferred to tubes for LC-MS analysis. A procedure blank was generated identically without plasma, which was used later to remove the background ions.

Tissue Metabolite Extraction. Mice were euthanized by injecting 120 mg/kg pentobarbital via an arterial catheter. All blood sampling was done before pentobarbital injection. Sodium pentobarbital 390 mg/mL (FATAL-PLUS SOLUTION, Vortech Pharmaceuticals, Ltd.) was diluted in sterile saline to obtain a 120 mg/mL working solution. For a 25-g mouse, 25 μL 120 mg/mL pentobarbital working solution was injected through the arterial catheter. The original FATAL-PLUS SOLUTION contains 29% v/v ethanol and 1% v/v propylene glycol. In the working solution, ethanol and propylene glycol concentrations are 8.9% v/v and 0.31% v/v, respectively. Tissues were quickly dissected and snap frozen in liquid nitrogen with a precooled Wollenberger clamp. Snap-frozen tissues were transferred to 2-mL round-bottom Eppendorf Safe-Lock tubes on dry ice. Samples were then ground into powder with a cryomill machine (Retsch) for 30 s at 25 Hz, and

maintained at a cold temperature using liquid nitrogen. For every 20 mg tissue, 800 μL −20 °C 40:40:20 (v/v/v) acetonitrile:methanol:water solution was added to the tube, vortexed for 10 s, and then centrifuged at 21,000 × g for 20 min at 4 °C. The supernatants were then transferred to plastic vials for LC-MS analysis. A procedure blank was generated identically without tissue and was used later to remove the background ions.

Metabolite Measurement by LC-MS. Metabolites were analyzed using a Vanquish Horizon UHPLC System (Thermo Scientific) coupled to an Orbitrap Exploris 480 mass spectrometer (Thermo Scientific). Waters XBridge BEH Amide XP Column [particle size, 2.5 μm; 150 mm (length) × 2.1 mm (i.d.)] was used for hydrophilic interaction chromatography (HILIC) separation. Column temperature was kept at 25 °C. Mobile phases A = 20 mM ammonium acetate and 22.5 mM ammonium hydroxide in 95:5 (v/v) water:acetonitrile (pH 9.45) and B = 100% acetonitrile were used for both ESI positive and negative modes. The linear gradient eluted from 90% B (0.0 to 2.0 min), 90% B to 75% B (2.0 to 3.0 min), 75% B (3.0 to 7.0 min), 75% B to 70% B (7.0 to 8.0 min), 70% B (8.0 to 9.0 min), 70% B to 50% B (9.0 to 10.0 min), 50% B (10.0 to 12.0 min), 50% B to 25% B (12.0 to 13.0 min), 25% B (13.0 to 14.0 min), 25% B to 0.5% B (14.0 to 16.0 min), 0.5% B (16.0 to 20.5 min), then stayed at 90% B for 4.5 min. The flow rate was 0.15 mL/min. The sample injection volume was 5 μL. ESI source parameters were set as follows: spray voltage, 3,200 V or −2,800 V, in positive or negative modes, respectively; sheath gas, 35 arb; aux gas, 10 arb; sweep gas, 0.5 arb; ion transfer tube temperature, 300 °C; vaporizer temperature, 35 °C. LC–MS data acquisition was operated under a full-scan polarity switching mode for all samples. The full scan was set as orbitrap resolution, 120,000 at m/z 200; AGC target, 1e7; maximum injection time, 200 ms; scan range, 60 to 1,000 m/z.

Data Analysis. LC-MS raw data files (.raw) were converted to mzXML format using ProteoWizard (version 3.0.20315) (34). El-MAVEN (version 0.12.0) (35) was used to generate a peak table containing m/z, retention time, and intensity for the peaks. Parameters for peak picking were the defaults except for the following: mass domain resolution, 5 ppm; time domain resolution, 10 scans; minimum intensity, 10,000; and minimum peak width, five scans. The resulting peak table was exported as a .csv file. Peak annotation of untargeted metabolomics data was performed using NetID (35) with default parameters. For tracer experiments, isotope labeling was corrected for 13C and 15N natural abundances using AccuCor2 package (36). Statistical analyses were performed using MetaboAnalyst 5.0 (37) and GraphPad Prism (version 9.0.0). Circulatory turnover fluxes and direct contribution of circulating nutrients to tissue TCA were calculated as previously described (24). In this analysis, sources of tissue TCA carbon were quantified by the fractional contribution of circulating 13C-glucose or 13C-lactate to tissue 4C units (malate and succinate). Such 4C-unit labeling also reflects 2C-unit sources, as i) even on the first turn of the TCA cycle, half of malate and succinate come from 2C units, and ii) TCA turning rather than anaplerotic flux predominates in most contexts (38).

Quantification of the Nutrient Turnover Fluxes. To measure the circulatory turnover flux of a nutrient with a carbon number of C, the uniformly ^{13}C-labeled form of the nutrient was infused. At steady state, the fraction of the labeled form $[M+i]$ of the nutrient in serum was measured as $L_{[M+i]}$. The circulatory turnover flux F_{circ} is defined as

$$F_{circ} = R \bullet \frac{1 - L_{[M+C]}}{L_{[M+C]}},$$

where R is the infusion rate of the labeled tracer (39).

Quantification of the Effect of Handling Stress. If we define $C_{(X,i)}$ as the relative concentration of a metabolite i from blood sampling site X (blood sampling site X = Artery 1 (A1) or Artery 2 (A2) or Tail (T)),

$$C_{(A1,i)} = I_{(A1,i)} / I_{(A1,i)} = 1,$$

$$C_{(A2,i)} = I_{(A2,i)} / I_{(A1,i)},$$

$$C_{(T,i)} = I_{(T,i)} / I_{(A1,i)},$$

where $I_{(X,i)}$ is the measured peak intensity of a metabolite i from blood sampling site X.

If we assume metabolite concentrations from Artery 2 are affected by handling stress while that from Tail are affected by both handling stress and arteriovenous difference,

$$S_{(i)} = C_{(A2,i)} - C_{(A1,i)},$$

$$AV_{(i)} = C_{(T,i)} - C_{(A2,i)},$$

where $S_{(i)}$ and $AV_{(i)}$ are the relative concentration change of a metabolite i due to handling stress and arteriovenous difference, respectively.

Data, Materials, and Software Availability. All study data are included in the article and/or *supporting information*.

ACKNOWLEDGMENTS. We thank the members of the J.D.R. laboratory for general assistance and discussions. W.D.L. is supported by NIH F32DK127843. J.D.R. is supported by NIH R01CA163591, NIH DP1DK113643, the Paul Allen Foundation, and Ludwig Cancer Research.

1. C. Gieger *et al.*, Genetics meets metabolomics: A genome-wide association study of metabolite profiles in human serum. *PLoS Genet.* **4**, e1000282 (2008).
2. L. Guoa *et al.*, Plasma metabolomic profiles enhance precision medicine for volunteers of normal health. *Proc. Natl. Acad. Sci. U.S.A.* **112**, E4901–E4910 (2015).
3. C. Menni *et al.*, Metabolomic markers reveal novel pathways of ageing and early development in human populations. *Int. J. Epidemiol.* **42**, 1111–1119 (2013).
4. K. Suhre *et al.*, Human metabolic individuality in biomedical and pharmaceutical research. *Nature* **477**, 54–62 (2011).
5. M. V. Milburn, K. A. Lawton, Application of metabolomics to diagnosis of insulin resistance. *Annu. Rev. Med.* **64**, 291–305 (2013).
6. E. Holmes, I. D. Wilson, J. K. Nicholson, Metabolic phenotyping in health and disease. *Cell* **134**, 714–717 (2008).
7. J. Ivanisevic *et al.*, Arteriovenous blood metabolomics: A readout of intra-tissue metabostasis. *Sci. Rep.* **51**, 1–13 (2015).
8. C. Jang *et al.*, Metabolite exchange between mammalian organs quantified in pigs. *Cell Metab.* **30**, 594–606.e3 (2019).
9. D. Murashige, Comprehensive quantification of fuel use by the failing and nonfailing human heart. *Science* **370**, 364–368 (2020).
10. J. Fernández-García, P. Altea-Manzano, E. Pranzini, S. M. Fendt, Stable isotopes for tracing mammalian-cell metabolism in vivo. *Trends Biochem. Sci.* **45**, 185–201 (2020).
11. C. R. Bartman, T. TeSlaa, J. D. Rabinowitz, Quantitative flux analysis in mammals. *Nat. Metab.* **37**, 896–908 (2021).
12. R. R. Wolfe, *Radioactive and Stable Isotope Tracers in Biomedicine: Principles and Practice of Kinetic Analysis* (Wiley, 1992).
13. J. P. Balcombe, N. D. Barnard, C. Sandusky, Laboratory routines cause animal stress. *Contemp. Top. Lab. Anim. Sci.* **43**, 42–51 (2004).
14. J. E. Ayala, D. P. Bracy, O. P. McGuinness, D. H. Wasserman, Considerations in the design of hyperinsulinemic-euglycemic clamps in the conscious mouse. *Diabetes* **55**, 390–397 (2006), 10.2337/diabetes.55.02.06.db05-0686.
15. K. A. Overmyer, C. Thonusin, N. R. Qi, C. F. Burant, C. R. Evans, Impact of anesthesia and euthanasia on metabolomics of mammalian tissues: Studies in a C57BL/6J mouse model. *PLoS One* **10**, e0117232 (2015).
16. Y. K. Chan *et al.*, Influence of tail versus cardiac sampling on blood glucose and lipid profiles in mice. *Lab. Anim.* **46**, 142–147 (2012).
17. S. Liu *et al.*, Long circulating tracer tailored for magnetic particle imaging. *Nanotheranostics* **5**, 348 (2021).
18. P. L. Debbage *et al.*, Lectin intravital perfusion studies in tumor-bearing mice: Micrometer-resolution, wide-area mapping of microvascular labeling, distinguishing efficiently and inefficiently perfused microregions in the tumor. *J. Histochem. Cytochem.* **46**, 627–639 (1998).
19. A. A. Boldyrev, G. Aldini, W. Derave, Physiology and pathophysiology of carnosine. *Physiol. Rev.* **93**, 1803–1845 (2013).
20. C. F. Huebner, E. Kodicek, K. K. Reddi, Carnosine phosphate as phosphate donor in muscular contraction. *Nature* **178**, 539–540 (1956).
21. K. M. Hanson, J. D. Simon, Epidermal trans-urocanic acid and the UV-A-induced photoaging of the skin. *Proc. Natl. Acad. Sci. U.S.A.* **95**, 10576–10578 (1998).
22. J. W. Pan, J. R. Hamm, D. L. Rothman, R. G. Shulman, Intracellular pH in human skeletal muscle by 1H NMR. *Proc. Natl. Acad. Sci. U.S.A.* **85**, 7836–7839 (1988).
23. G. A. Brooks *et al.*, The blood lactate/pyruvate equilibrium affair. *Am. J. Physiol. Endocrinol. Metab.* **322**, E34–E43 (2022).
24. S. Hui *et al.*, Glucose feeds the TCA cycle via circulating lactate. *Nature* **551**, 115–118 (2017).
25. J. C. Preiser, C. Ichai, J. C. Orban, A. B. J. Groeneveld, Metabolic response to the stress of critical illness. *Br. J. Anaesth.* **113**, 945–954 (2014).
26. L. Wecker, *Brody's Human Pharmacology* (Elsevier Health Sciences, 2018) (September 25, 2022).
27. K. Farzam, A. Kidron, A. D. Lakhkar, *Adrenergic Drugs* (StatPearls Publishing LLC., 2022).
28. R. S. Sherwin, L. Sacca, Effect of epinephrine on glucose metabolism in humans: Contribution of the liver. *Am. J. Physiol.* **247**, E157–E165 (1984), 10.1152/ajpendo.1984.247.2.E157.
29. T. TeSlaa *et al.*, The source of glycolytic intermediates in mammalian tissues. *Cell Metab.* **33**, 367–378.e5 (2021).

30. J. Jensen, P. I. Rustad, A. J. Kolnes, Y. C. Lai, The role of skeletal muscle glycogen breakdown for regulation of insulin sensitivity by exercise. *Front. Physiol.* **2**, 112 (2011).
31. V. Qvisth, E. Hagström-Toft, S. Enoksson, J. Bolinder, Catecholamine regulation of local lactate production in vivo in skeletal muscle and adipose tissue: Role of β-adrenoreceptor subtypes. *J. Clin. Endocrinol. Metab.* **93**, 240–246 (2008).
32. D. C. Nieman, K. A. Carlson, M. E. Brandstater, R. T. Naegele, J. W. Blankenship, Running endurance in 27-h-fasted humans. *J. Appl. Physiol.* **63**, 2502–2509 (1987), 10.1152/jappl.1987.63.6.2502.
33. M. H. Vendelbo *et al.*, Insulin resistance after a 72-h fast is associated with impaired AS160 phosphorylation and accumulation of lipid and glycogen in human skeletal muscle. *Am. J. Physiol. - Endocrinol. Metab.* **302**, 190–200 (2012).
34. M. C. Chambers, A cross-platform toolkit for mass spectrometry and proteomics. *Nat. Biotechnol.* **30**, 918–920 (2012).
35. S. Agrawal *et al.*, El-MAVEN: A fast, robust, and user-friendly mass spectrometry data processing engine for metabolomics. *Methods Mol. Biol.* **1978**, 301–321 (2019).
36. Y. Wang, L. R. Parsons, X. Su, AccuCor2: Isotope natural abundance correction for dual-isotope tracer experiments. *Lab. Investig.* **101**, 1403–1410 (2021).
37. Z. Pang *et al.*, Using MetaboAnalyst 5.0 for LC–HRMS spectra processing, multi-omics integration and covariate adjustment of global metabolomics data. *Nat. Protoc.* **17**, 1735–1761 (2022).
38. C. R. Bartman *et al.*, Slow TCA flux and ATP production in primary solid tumours but not metastases. *Nature* **614**, 349–357 (2023).
39. S. Hui *et al.*, Quantitative fluxomics of circulating metabolites. *Cell Metab.* **32**, 676–688.e4 (2020).